Acta Pharmaceutica Sinica B 2019;9(2):294–303

Chinese Pharmaceutical Association
Institute of Materia Medica, Chinese Academy of Medical Sciences

Acta Pharmaceutica Sinica B

www.elsevier.com/locate/apsb
www.sciencedirect.com

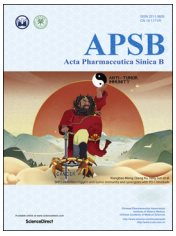

ORIGINAL ARTICLE

Glycyrrhetinic acid binds to the conserved P-loop region and interferes with the interaction of RAS-effector proteins

Yuan Zhang, Zhihua Wang, Xiaoyao Ma, Shengnan Yang, Xueyan Hu, Jin Tao, Yuanyuan Hou*, Gang Bai*

State Key Laboratory of Medicinal Chemical Biology, College of Pharmacy and Tianjin Key Laboratory of Molecular Drug Research, Nankai University, Tianjin 300353, China

Received 7 August 2018; received in revised form 25 October 2018; accepted 26 October 2018

KEY WORDS

Glycyrrhetinic acid;
RAS;
Allosteric inhibitor;
RAS/MAPK signalling

Abstract Members of the *RAS* proto-oncogene superfamily are indispensable molecular switches that play critical roles in cell proliferation, differentiation, and cell survival. Recent studies have attempted to prevent the interaction of RAS/GTP with RAS guanine nucleotide exchange factors (GEFs), impair RAS-effector interactions, and suppress RAS localization to prevent oncogenic signalling. The present study aimed to investigate the effect of the natural triterpenoic acid inhibitor glycyrrhetinic acid, which is isolated from the roots of *Glycyrrhiza* plant species, on RAS stability. We found that glycyrrhetinic acid may bind to the P-loop of RAS and alter its stability. Based on our biochemical tests and structural analysis results, glycyrrhetinic acid induced a conformational change in RAS. Meanwhile, glycyrrhetinic acid abolishes the function of RAS by interfering with the effector protein RAF kinase activation and RAS/MAPK signalling.

Abbreviations: CD, circular dichroism; DTT, D,L-dithiothreitol; FTIs, farnesyltransferase inhibitors; FTS, fluorescence-based thermal shift; GA, glycyrrhetinic acid; GAPs, GTP hydrolysis by GTPase-activating proteins; GEFs, guanine nucleotide exchange factors; HOBt, hydroxybenzotrizole; Kobe, Kobe0065; N_3-tag, 3-azido-7-hydroxycoumarin; NH_2-MMs, Fe_3O_4 amino magnetic microspheres; RAS, GTPases RAS; SPR, surface plasmon resonance; Sulfo-SADP, sodium1-((3-((4-azidophenyl)disulfanyl)propanoyl)oxy)-2,5-dioxopyrrolidine-3-sulfonate; Tip, tipifarnib

*Corresponding authors. Tel./fax: +86 22 23506792.
E-mail addresses: houyy@nankai.edu.cn (Yuanyuan Hou), gangbai@nankai.edu.cn (Gang Bai).

Peer review under responsibility of Institute of Materia Medica, Chinese Academy of Medical Sciences and Chinese Pharmaceutical Association.

https://doi.org/10.1016/j.apsb.2018.11.002

1. Introduction

RAS GTPases (RAS) are signal transduction pathway regulators that control cell proliferation, survival, differentiation, and apoptosis[1–3]. The RAS protein is an intracellular guanine nucleotide-binding protein (G protein) that comprises two domains: The G domain and the hypervariable region. The G domain binds guanine nucleotides and comprises three dynamic structural motifs: switch I (residues 30–38), switch II (residues 60–76), and the phosphate-binding (P)-loop (residues 10–17). The switch I and II motifs constitute the nucleotide-binding site and interfaces for downstream effectors[4,5]. The P-loop regulates vital interactions with the phosphate groups of nucleotides[6–8]. Normally, RAS activity is regulated by a switch between the GTP-bound state (ON) and the GDP-bound state (OFF) following GTP hydrolysis by GTPase-activating proteins (GAPs)[9] or acceleration of GDP release and GTP binding by guanine nucleotide exchange factors (GEFs, such as SOS)[10]. Consequently, small-molecule inhibitors selectively maintain the OFF conformation to inhibit RAS signalling by disrupting the binding of either effectors[11].

RAS mutations have been reported in over 30% of solid tumours and in approximately 20% of common myeloid malignancies, particularly in pancreatic, lung, and colon cancers[12]. These mutations are often tumorigenic and inhibit the GTPase activity of RAS, resulting in the accumulation of activated RAS. In particular, RAS mutations have been shown to inhibit the interaction of RAS with GAPs, thereby decelerating the rate of hydrolysis and accelerating the activation of GTP-bound effectors such as PI3K[13], RAF[14], and RalGDS[15], thereby affecting the cytoskeletal organization, transcriptional regulation, or membrane trafficking pathways in the cell[16].

RAS inhibitors are difficult to establish due to the lack of well-defined surface pockets that facilitate drug binding[17,18]. Recent studies have identified certain small molecules that directly inhibit and disrupt crucial functions of RAS. For example, andrographolide and its derivative (SRJ23) inhibit GDP–GTP exchange and abrogate the interactions of oncogenic RAS with its effectors[19]. Some mutant-specific inhibitors form covalent bond with the thiol of the G12C cysteine residue in the P-loop, which constitutively activate RAS through locked GTP binding[20]. The study by Gentile et al.[21] utilized disulphide tethering of a non-natural cysteine (K-RAS (M72C)) to identify a new switch-II pocket (S-IIP) binding ligand (2C07) that engages the active GTP state. FarnesyltransfeRASe inhibitors (FTIs) target the CAAX motif in RAS and prevent membrane binding of RAS[22,23]. Despite previous efforts, anti-RAS therapies have not been implemented in the clinical setting.

Glycyrrhetinic acid (GA), a triterpenoic acid derived from the roots of the *Glycyrrhiza* plant, has widespread clinical applications due to its anti-allergic[24], hepatoprotective, anti-inflammatory, antimicrobial, and antitumour effects[25,26]. From in our previous study, GA exerts a synergistic anti-asthmatic effects *via* a β2-adrenergic receptor-mediated pathway[27]. In the present study, chemical biology strategies were primarily used to identify potential target proteins of GA. The RAS protein was evaluated as a potential target of GA using fluorescence-based thermal drift (FTS) and surface plasmon resonance (SPR) analyses. In addition, negative-staining electron microscopy and SPR analyses of the interaction between GA and the wild-type or mutant H-RAS protein revealed that GA binds to the P-loop of RAS, triggers a conformational change, impairs RAS interaction with its effector proteins, and disrupts oncogenic RAS function.

2. Materials and methods

2.1. Reagents, cell culture, SDS-PAGE, and Western blotting

A549 (human adenocarcinoma cells) and HepG2 (hepatocellular carcinoma cells) cell lines were obtained from American Type Culture Collection (Manassas, VA, USA). Cell lines were tested for murine pathogens and mycoplasma and found to be negative. A549 and HepG2 cell lines were maintained in Dulbecco's modified Eagle's medium (DMEM) supplemented with 10% (*v*/*v*) foetal bovine serum and 100 unit/mL penicillin and incubated at 37 °C in a 5% CO_2 atmosphere. Western blot and SDS-PAGE analyses are consistent with the literature[28] using the antibodies anti-RAS (3965), anti-P38 (9212), anti-phospho-P38 (9211), anti-ERK1/2 (9102), anti-phospho-ERK1/2 (4370), anti-GAPDH (2118), and a goat anti-rabbit IgG (7074) secondary antibody, which were purchased from Cell Signaling Technology (Beverly, MA, USA). C-RAF (3965), phospho-c-RAF (S338, 9427, S259, ab173539), phospho-B-RAF (S729, ab124794, T401, ab68215), and Alexa Fluor 594-conjugated goat anti-rabbit IgG (ab150084) were purchased from Abcam (Cambridge, UK). The HRAS-c-RAF inhibitor Kobe0065 (Kobe) and farnesyltransferase (FTase) inhibitor tipifarnib (Tip) were purchased from Selleck (Houston, Texas, USA). Kobe is a RAS family small GTPase inhibitor that inhibits the interaction of RAS/GTP with multiple effectors, including RAF, PI3K, and RalGDS and SOS[29]. Tip can inhibit the prenylation of the CAAX tail motif of FTase, which allows RAS to bind to the membrane[30]. Glycyrrhetinic acid (purity > 98.5%, as determined by HPLC) and propargylamine were purchased from J&K Chemical (Beijing, China).

2.2. Enrichment of target proteins in cells

A549 cells were cultured with 10 μmol/L alkynyl-GA probe for 6 h. After three washes with precooled PBS, 500 μL of lysis buffer (Solarbio, Beijing, China) was added and incubated on ice. Cell lysates were then treated with GA-modified functionalised magnetic microspheres (probe 1) and incubated with a catalyst (2.0 mmol/L sodium ascorbic acid and 1.0 mmol/L $CuSO_4$ in precooled PBS) overnight at 4 °C. Afterwards, probe 1 was separated with magnets and washed by PBS. Enriched probe 1 was then treated with D,L-dithiothreitol (DTT) (100 mmol/L) to release the captured protein targets. Then SDS-PAGE and Western blotting were performed in accordance with a previously reported method[28].

2.3. Co-localization of target proteins and GA

A549 cells were cultured in flasks with 1 μmol/L alkynyl-GA probe. After washing, fixation with 4% paraformaldehyde, and blocking with 10% goat serum, anti-RAS antibodies (1:1000) were added and incubated overnight at 4 °C. Afterwards, Alexa Fluor 594-conjugated secondary antibodies (1:1000) were added to the cells and incubated for 1 h at room temperature. The N_3-tag substrate (10 μmol/L) was then added to the cells for the probe 2 click reaction with the aforementioned catalyst system. After an adequate number of washes, fluorescence images were obtained with a confocal microscope (Leica TCS SP8, Japan): Alexa Fluor594: λ_{Ex}: 594 and λ_{Ee}: 617 nm; probe 2: λ_{Ex}: 488 and λ_{Ee}: 520 nm. DAPI (1:1000) was used to stain the nucleus and images were captured at λ_{Ex}: 405 and λ_{Ee}: 430 nm.

2.4. Evaluation of RAS activation

A New East Assay Kit (NewEast Biosciences, Wuhan, China) was used for RAS detection according to the manufacturer's instructions. We appended a brief explain in the Supporting Information.

2.5. Fluorescence-based thermal shift (FTS) assay

The recombinant H-RAS protein, GA and Tip were diluted in their corresponding incubation buffers. The H-RAS protein was complexed with each compound at a 1:10 ratio (protein concentration, 10 μmol/L) and the Protein Thermal Shift Dye Kit™ (1:6000) in a total volume of 20 μL in a 96-well plate. Scanning (37–95 at 0.03 °C/s) was conducted by a real-time PCR machine (LightCycler®96, Roche, Switzerland). Data collection and organization are consistent with the literature[31].

2.6. Surface plasmon resonance (SPR) analysis of H-RAS

SPR experiments of the interaction of H-RAS with GA were performed by a Biacore T200 optical biosensor (GE Healthcare, Pittsburgh, PA, USA). Immobilization of recombinant wild-type or mutant H-RAS protein (50 μg/mL) was carried out in sodium acetate buffer (pH 5.5). During each binding cycle, the GA solution (1.9 to 250 μmol/L) was injected at a flow rate of 30 μL/min for 1 min and the dissociation was monitored for 300 s. Data collection and organization are consistent with the literature[31].

2.7. Negative stain electron microscopy

Briefly, the uranyl formate staining process is consistent with the literature[32]. Images were obtained from a Gatan 1400 TEM operated at 120 kV (Talos F200C, Waltham, MA, USA), using a 4 × 4 k CCD camera with a nominal magnification of 30 k, corresponding to 3.71 Å/pixel. Defocus value ranged between 1 and 2 μm.

2.8. Circular dichroism (CD) spectroscopy

The purified H-RAS protein was dialyzed against sodium phosphate buffer (pH 7.4). CD spectral analysis was performed at 20 °C using a MOS-450 spectropolarimeter (Bio-Logic, France) equipped with a Peltier unit for temperature control.

2.9. Migration and invasion assays

A549 cells were treated with various concentrations of GA (20 or 40 μmol/L) or Tip (10 μmol/L) and cultured for 24 h in 24-well plates in the upper wells of transwell migration inserts and transwell BD BioCoat™ Matrigel™ invasion chambers (pore size: 8 μm, BD Biosciences, Franklin Lake, New Jersey, USA). Cells that had migrated and invaded the lower surface were stained with crystal violet and then enumerated manually.

2.10. Cell cycle analysis

The A549 cells were incubated with certain concentrations of GA, kobe and Tip for 24 h. Then, the cells were harvested and fixed in ice-cold 70% (*v*/*v*) ethanol overnight at −20 °C. The cell pellet was resuspended in PBS and stained with a mixture of RNase (10 μg/mL) and PI (25 mg/mL) in sodium citrate containing 0.5% Triton X-100 for 30 min in the dark. Fluorescence was measured using a flow cytometer (BD LSRFortessa, Franklin Lake, New Jersey, USA).

2.11. Xenografts in nude mice

Six-week-old female BALB/c nude mice (specific pathogen-free [SPF]) were purchased from the Laboratory Animal Experimental Center of Academy of Military Medical Sciences (No. 1601563; Beijing, China). Studies using experimental animals were performed according to protocols approved by Nankai University Ethics Committee on Pre-Clinical Studies. A549 cells (1×10^7) were subcutaneously (s.c.) injected into the right flanks of the mice. The mice were randomly assigned to 4 groups ($n = 6$ mice per group): two groups were intragastrically (i.g.) administered GA (50 or 100 mg/kg) daily for 40 days, and one group was i.g. administered Kobe (80 mg/kg) daily. Tumour volumes (V) were calculated using previously described methods[33].

2.12. H&E and IHC staining

Tumour tissue sections were deparaffinised, rehydrated, and boiled in sodium citrate for 15 min for antigen retrieval. After quenching endogenous peroxidases, sections were incubated with an anti-P-ERK1/2 antibody (1:500) overnight at 4 °C. Alexa Fluor 594-conjugated goat anti-rabbit IgG (1:1000) was applied to the sections and incubated at 37 °C for 45 min. Fluorescence images were generated with a confocal microscope (Leica TCS SP8).

2.13. Statistical analysis

The results were reported as means ± S.D. (standard deviations). For single comparisons, significant differences between the means were determined using Student's *t*-test. A *P*-value less than 0.05 was regarded as indicate significant differences. All data were processed using the GraphPad Prism statistical software, version 5.01 (La Jolla, CA, USA).

3. Results

3.1. In silico docking and target fishing of GA probe

To screen for potential targets of GA, a virtual docking process was adopted using PhamMapper (http://59.78.96.61/phammapper). The first 40 candidate targets of GA are listed in Supporting Information Table S1. Next, we studied the candidate targets by putting them into String 10.0 (http://www.string-db.org/) and found that RAS was involved in the MAPK signalling pathway and constitutes the RAS/RAF/MEK/ERK axis (Supporting Information Fig. S1). Then, the candidate targets were selected and assessed used AutoDock and Molecular Operating Environment software (Supporting Information Fig. S2). The binding energies of GA targeting MAP2K1, PKCα, MAPK14, MAPK10, H-RAS and MAPK1 were found to be –9.93, –8.77, –8.82, –7.93, –7.47 and –7.36 kcal/mol, respectively.

To validate the results of this *in silico* analysis, alkynyl-GA was synthesized according to the scheme shown in Fig. 1A. To identify

the potential targets, the GA-modified functionalized MMs (probe 1) were used to capture protein targets in A549 cells. The captured proteins were released by DTT reduction (Fig. 1B). To assess collection efficiency, SDS-PAGE and Western blotting were then performed. Levels of the RAS protein, which was presented as an approximately 21 kDa band, were significantly increased in the probe 1-enriched microspheres compared with the non-alkynyl-GA-modified microspheres in the control group (Fig. 1C, right and left panel). Meanwhile, we performed capture capacity assays for other targets. The result is shown that MAPK1, MAPK14 and PKCα were also captured in the same system as the RAS protein. However, JNK and MEK1 did not yield clear positive results (Supporting Information Fig. S3). Since MAPK1, MAPK14 and PKCα are located downstream of the RAS signalling pathway. Therefore, the goal of GA is still focused on the RAS protein. Next, tracking probe 2 was synthesized (Fig. 1D). As expected, the click product probe 2 showed strong fluorescence, while the three substrates (alkynyl-GA, GA and N_3-tag) showed almost no fluorescence (Fig. 1E). Under identical conditions, analysis of co-localization of alkynyl-GA probe and the RAS protein expression by confocal microscopy on A549 cells. The GA (10 µmol/L) treatment group showed little

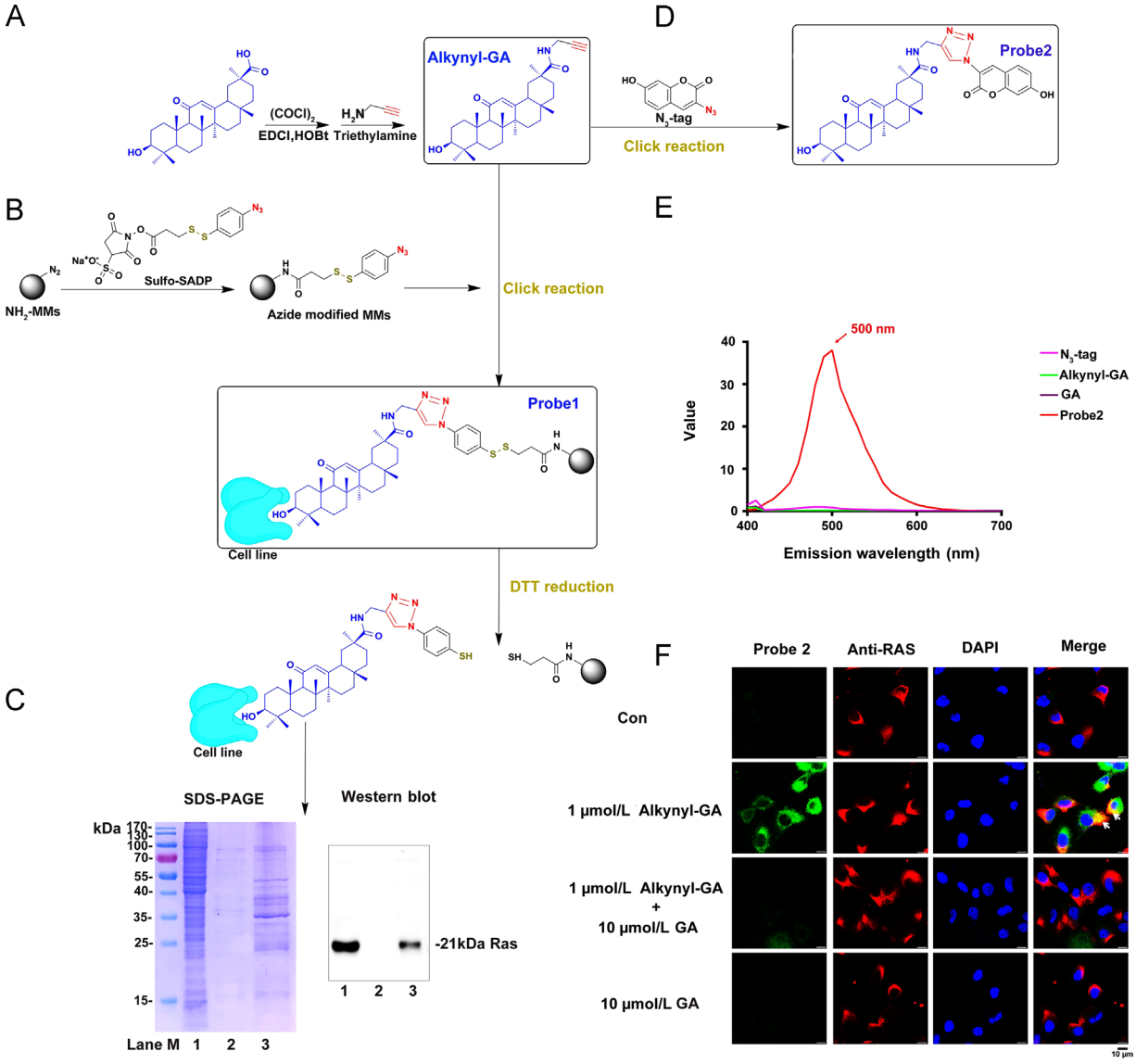

Figure 1 GA targets RAS and co-localizes with RAS in A549 cells. (A) Synthesis of alkynyl-modified GA (alkynyl-GA). (B) Synthesis of GA-modified functionalized MMs (probe 1) and the process for capturing and releasing the target protein. (C) Lane 1 shows A549 lysate as a loading control, Lane 2 shows the lysate captured by the azide-modified MMs as a negative control, and Lane 3 shows the lysate captured by probe 1. Markers indicate the molecular weight. The concentrations of all protein samples were adjusted to equal amounts before capture and were adjusted to the same volume after capture for SDS-PAGE and Western blot analyses. (D) Synthesis of fluorescent click product (probe 2). (E) Fluorescence intensity of the click product (probe 2) compared with alkynyl-GA, GA and N_3-tag. (F) Analysis of the co-localization of alkynyl-GA and the RAS protein using fluorescence confocal microscopy. The GA (10 µmol/L) treatment group showed little fluorescence. But obvious alkynyl-GA (1 µmol/L) fluorescence was observed in the cytoplasm (green). The specific fluorescence was competitively ablated by a 10 µmol/L GA treatment. Alexa Fluor594 staining for RAS (red) was found in the cytoplasm and membrane and partially co-localized with alkynyl-GA (yellow), as indicated by the arrows, scale bar 10 µm.

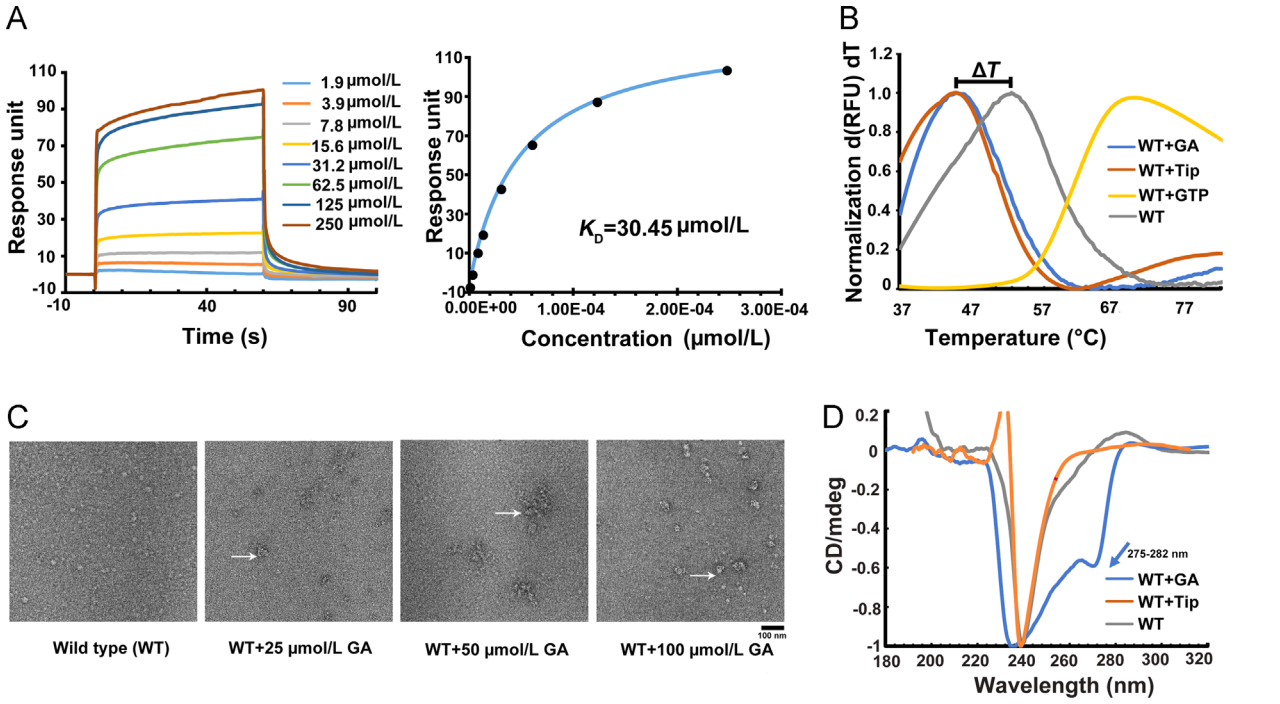

Figure 2 GA binds to RAS and changes its conformational state. (A) SPR analysis of interactions between GA and H-RAS. A Biacore CM5 chip was used to capture H-RAS. Measures of GA/RAS association and dissociation were performed in the presence of various GA concentrations ranging from 1.9 to 250 μmol/L. After passage over the surface of the CM5 chip, an apparent K_D of 30.45 μmol/L was obtained. (B) The thermal stability of the H-RAS protein incubated with GA was assessed using the thermal shift assay. (C) Negative stain electron microscopy analysis of changes in wild-type H-RAS morphology before and after treatment with 25, 50 and 100 μmol/L GA. Arrows indicate irregular oligomers of the RAS protein, scale bar: 100nm. (D) The conformational state of the H-RAS protein (40 μmol/L) was analysed by CD after treatment with 400 μmol/L GA or 400 μmol/L Tip.

fluorescence. But obviously alkynyl-GA (1 μmol/L) fluorescence was observed in the cytoplasm. In addition, the specific fluorescence was competitively ablated by a 10 μmol/L GA treatment (Fig. 1F). This phenomenon indicated the specificity of the cytochemical staining for GA. The routes used by synthesize alkynyl-GA, probe 1 and probe 2 are shown in the supplementary data (Supporting Information Figs. S4–S8).

3.2. *GA binds to RAS and changes its conformational state*

To further evaluate the feasibility of GA combining with RAS as a ligand, adopting the conventional SPR tests to verify the binding of GA to RAS targets. Depending on SPR results, GA bound to the immobilized H-RAS protein and the binding affinities of GA was 30.45 μmol/L (Fig. 2A). Then, the FTS assay was conducted to assess H-RAS thermal stability upon GA binding. The principle of FTS assay measurement is that ligand binding changes the thermal stability of proteins[34]. Purified H-RAS protein was subjected to FTS in the presence and absence of GA (Fig. 2B). Strikingly, GA caused a 6–8 °C decrease in the protein melting temperature (Δ*T*), which was strongly suggesting that considerable conformational changes occurred in H-RAS upon GA binding and similar to the FTIs tipifarnib (Tip) control group. In contrast, treatment with the positive control GTP substantially increased H-RAS thermal stability and caused 15 °C increase in Δ*T*. Furthermore, the leftward shift always indicates substantial instability[31]. In addition, a negative stain electron microscopy experiments were performed to verify the binding of GA to H-RAS target. Electron microscopic observation of wild-type H-RAS protein was homogenously distributed. However, the H-RAS protein formed many irregular aggregates after incubation with GA, and these irregular aggregates existed in a dose-dependent manner (Fig. 2C). To confirm the sensitive conformation alterations induced by hydrophobic amino acid residues, circular dichroism (CD) spectroscopy was performed (Fig. 2D). After charging with GA, the CD spectra exhibited a slight change at approximately 275–282 nm. The region represented the specific absorbance of tyrosine residues[35]. The result indicated that GA displayed the greatest impact on the stability of H-RAS. The H-RAS protein expression and purification process are shown in the supplemental data (Supporting Information Fig. S9).

3.3. *GA targets the P-loop region of H-RAS*

For predicting the position of GA might bind in the RAS-GTP binding pocket, multiple molecular dynamics simulations of RAS (PDB ID codes 4EFL, 3 × 1W, and 2CL7) complexed with GA were conducted (Supporting Information Fig. S10). The predicted ligand binding site involves two distinct Pockets: Pocket 1, which includes the effector P-loop (residues 12–15), and Pocket 2, which includes switch II (residue 60). The P-loop is very important for binding nucleotides mainly binds to the β-phosphate of GDP and the β,γ-phosphates of GTP[36,37]. The predicted ligand binding site involves residues G12, G13 and G15 that possibly make hydrogen bonds with GA (Fig. 3A, right panel), which is identical to the GDP pocket (G13, G15, G16 and G17) (Fig. 3A, left panel). To verify the reliability of predicted amino acid sites, we prepared H-RAS mutants, which harboured alanine substitution at G12, G13, V14, G15 and G60, to examine ligand binding capacity using SPR approach[38]. Usually, alanine replaced proteins are used to identify residues important for protein stability, function and shape[39].

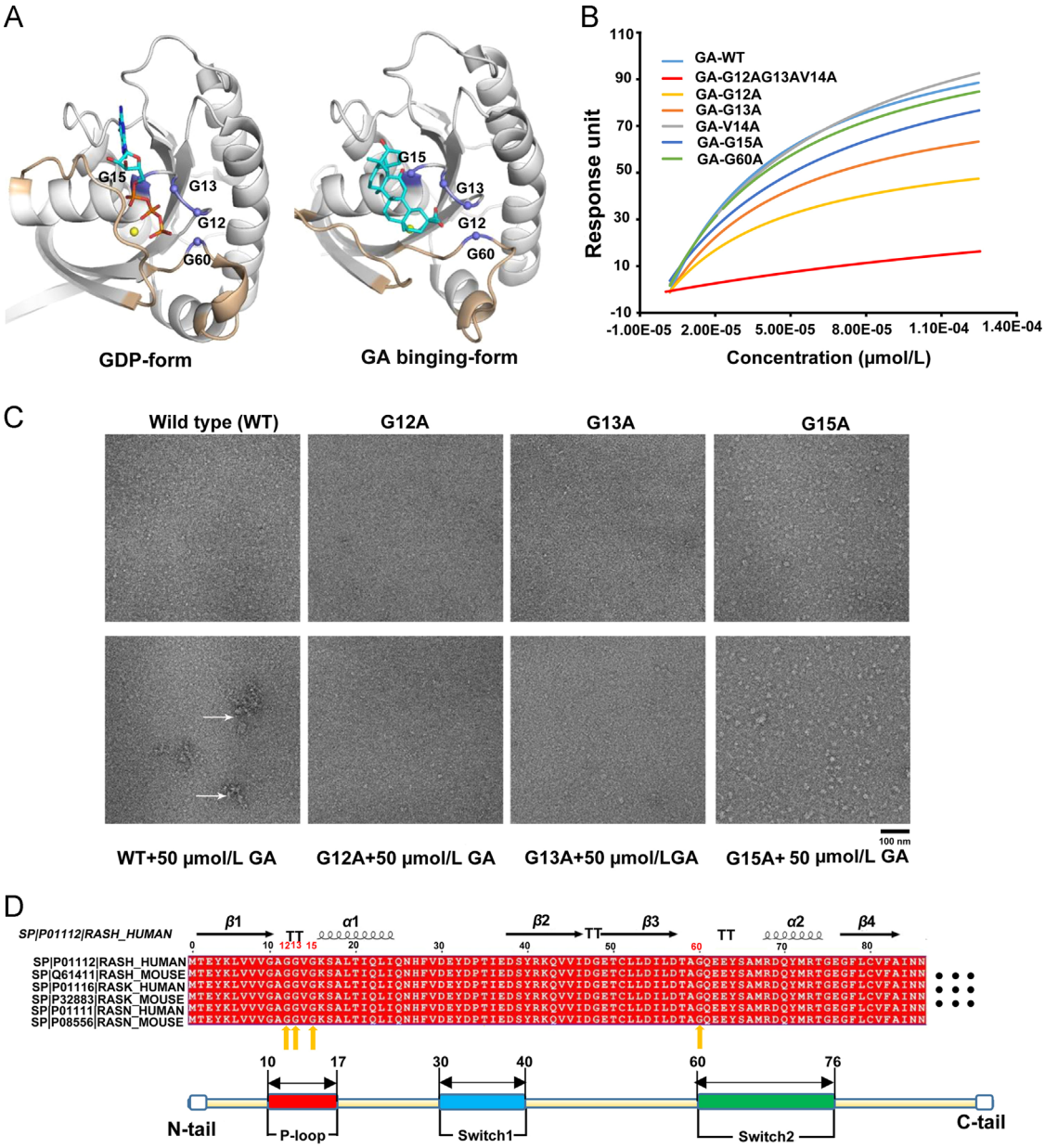

Figure 3 GA targets the P-loop region of RAS. (A) Molecular docking analysis of GDP and GA. A detailed docking model for H-RAS showed that carbonyl and hydroxide radicals in the GA structure form hydrogen bonds with Gly12, Gly13, Gly15, and Gly60. GDP was also docked into the P-loop pocket. (B) SPR response of GA incubated with different H-RAS mutant proteins. (C) Negative stain electron microscopy analysis of changes in wild-type and mutant H-RAS before and after treatment with 50 μmol/L GA. Arrows indicate the irregular oligomers of the RAS protein, scale bar: 100 nm. (D) Comparison of the main sequence of human and mouse members of the RAS family.

Compared to the wild-type protein, a mutation at G12, G13 and G15 resulted in nearly 60%, 50% and 40% loss of binding of GA, respectively. And multipoint mutations at G12/G13/V14 resulted in nearly lose binding of GA (Fig. 3B and Supporting Information Fig. S11). Furthermore, the negative stain electron microscopy of wild-type and mutant H-RAS with GA was carried respectively. As showed in Fig. 3C, the binding of GA strongly induced irregular aggregates of the wild-type H-RAS, and the irregular aggregate state was observed reduction for three mutants G12A, G13A and G15A. Taken together, these results suggested that GA interacts with the nucleotides binding region P-loop of H-RAS through specific residues and triggers H-RAS irregular aggregates. P-loop sequence is highly conserved across not only the H-RAS but also the whole RAS family (H-RAS, K-RAS and N-RAS) (Fig. 3D). These key basic residues (G12, G13, and G15) are reported to play essential roles in GTP-hydrolysis[40]. It is speculated that GA targets the P-loop and might affect all RAS family proteins normal functions.

3.4. GA inhibits the action of RAS and affects the function of downstream effectors

Normally, GTP binds to activate RAS and is inactivated when GTP is hydrolyzed to GDP. To further confirm the inhibitory effect of GA on RAS protein, a RAS activation assay kit was used

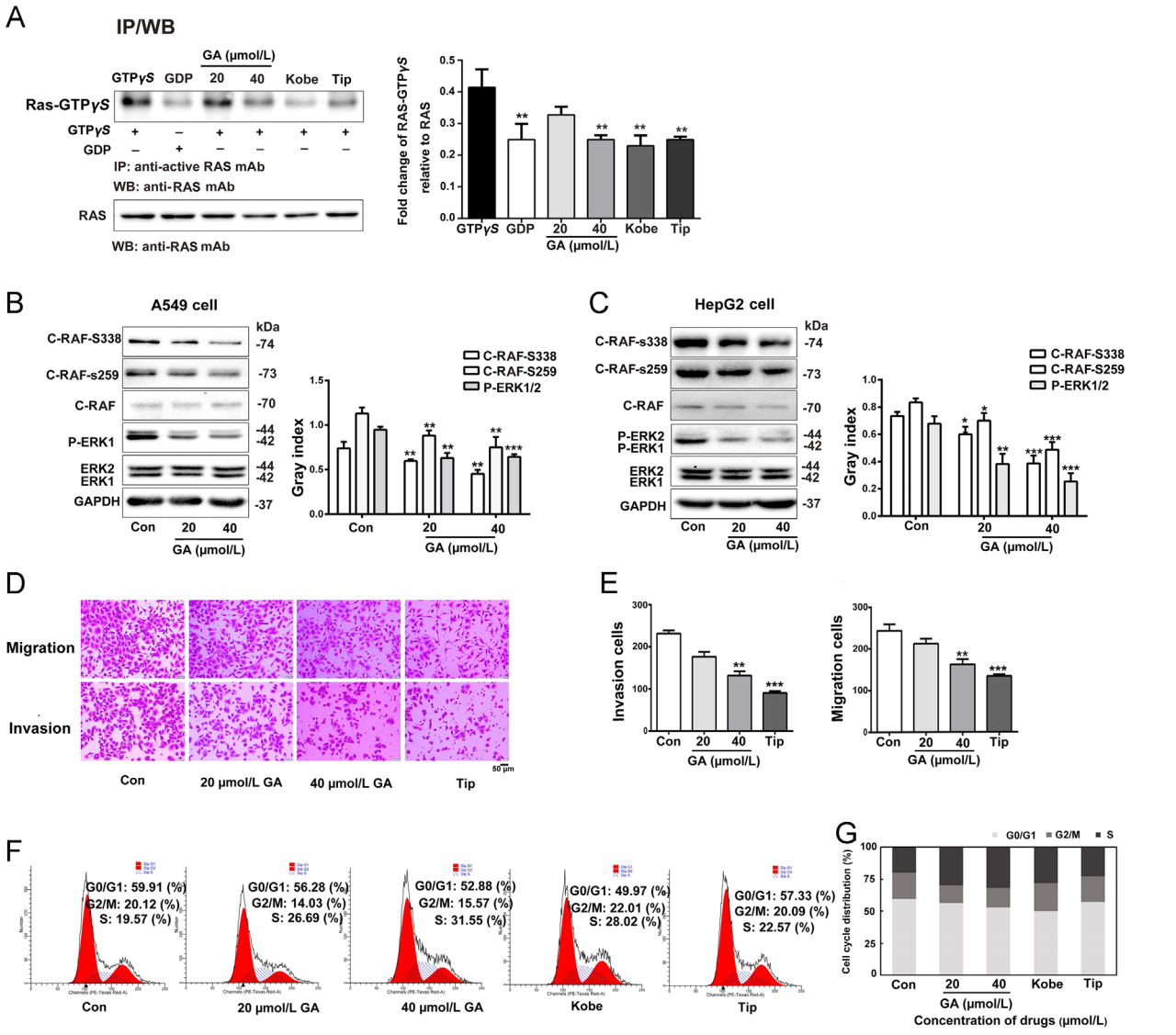

Figure 4 GA inhibits GTP binding and the activation of downstream effectors. (A) GA dose-dependently inhibits GTP binding and the activation of downstream effectors *in vitro*. (B) and (C) Western blots showing the levels of activated downstream effectors, c-RAF phosphorylated at S338 and S259 and phosphorylated ERK1/2 levels, in A549 cells and HepG2 cells after GA treatment. GAPDH expression was used as an internal control for normalization. The assay was performed three times, Error bars indicate means ± S.D. ($^{*}P < 0.05$, $^{**}P < 0.01$, $^{***}P < 0.001$ compared to the control). (D) and (E) A549 cells were cultured with 20 or 40 μmol/L GA. Migration (upper panel) and invasion (lower panel) were investigated using Transwell and Matrigel assays ($n = 5$), scale bar: 50 μm. (F) and (G) PI staining was performed to investigate the effect of GA on the cell cycle. Cells were treated with GA (20 or 40 μmol/L) for 24 h and then stained with PI. GA induced S phase arrest in A549 cells. Histogram shows the percentage of cells in G0/G1, G2/M and S Phase ($n = 3$).

to measure active RAS-GTP levels based on the use of a configuration-specific anti-RAS-GTPγS monoclonal antibody, then the bound active RAS was pulled down by protein A/G agarose. The precipitated active RAS was detected by immunoblot analysis using anti-RAS antibody. As showed in Fig. 4A, 40 μmol/L GA significantly inhibited intermolecular interactions of activation on A549 cells. RAS regulates proliferation by activating the mitogen-activated protein (MAP) kinase (ERK) cascade[41,42]. The first step in RAS-dependent activation of ERK signalling is RAS binding to members of the RAF family[43,44]. RAF kinase is a key RAS effector protein and is phosphorylated by RAS at residues S338 and S259[45]. Therefore, phosphorylated c-RAF and ERK1/2 were tested in A549 cells and HepG2 cells. c-RAF and ERK1/2 expression exhibited no evident changes, but the level of phosphorylation c-RAF at both Ser338 and Ser259 sites and the level of phosphorylation ERK1/2 were decreased following GA treatment in a dose-dependent manner (Fig. 4B and C).

3.5. *GA decreases cell migration, invasion, and inhibits cell cycle progression*

To assess the function of GA on the chemotactic motility of cancer cells *in vitro,* the effects of GA on cell migration and invasion were examined. Compared with the untreated control, the population of migrating cells decreased by 23.74% and 43.29% and the

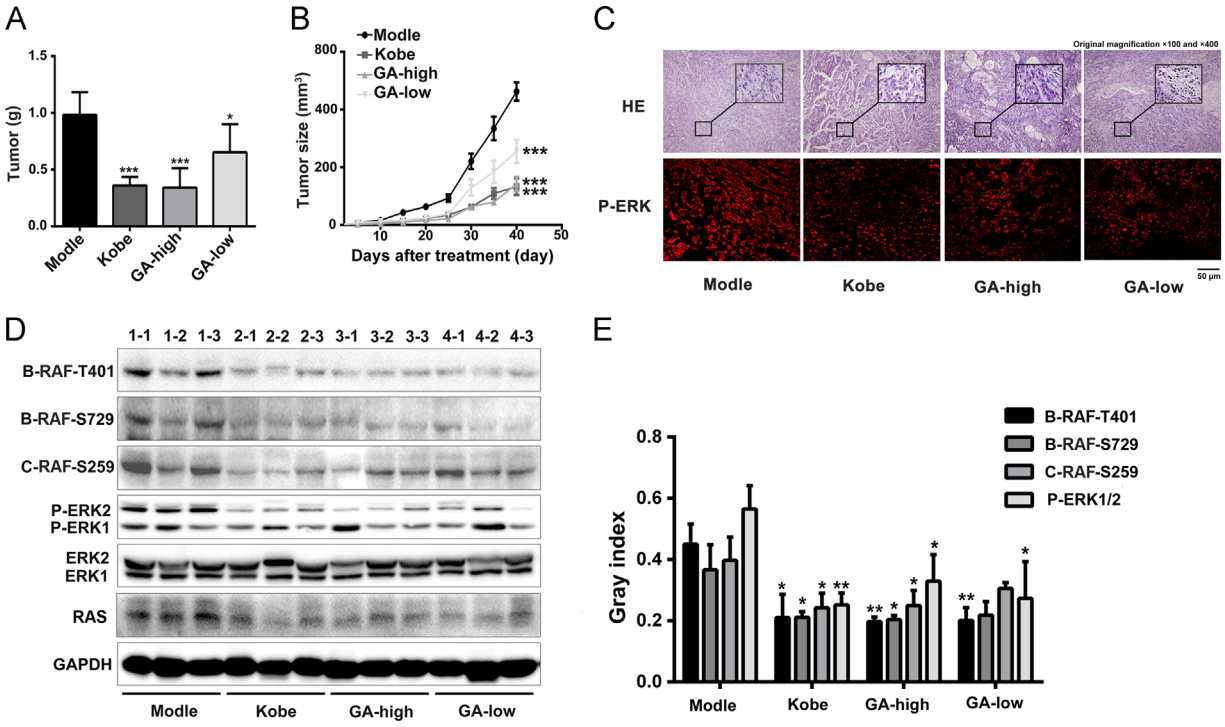

Figure 5 Treatment with GA inhibited the growth of A549 cells *in vivo*. (A) and (B) The GA treatment suppressed the formation of tumours by A549 cells *in vivo*. Mice were treated with 0.9% NaCl (model), GA (high dose, 100 mg/kg; low dose, 50 mg/kg) or Kobe (80 mg/kg). (A) Tumour weights were monitored. (B) Growth curves of the xenograft tumours. Values are presented as means ± S.D. ($n = 6$). (C) Images of H&E (original magnification × 100 and × 400), and IHC staining of the tumour tissues show the levels of P-ERK1/2, scale bar: 50 μm. (D) and (E) Levels of the phosphorylated c-RAF-S259, B-RAF-S729, B-RAF-T401 and ERK1/2 proteins in the tumour tissues were analysed by Western blotting. The data are reported as means ± S.D. ($n = 3$). $^{*}P < 0.05$, $^{**}P < 0.01$, $^{***}P < 0.001$ compared to the model.

population of invasive cells decreased by 12.76% and 33.33% following treatment with 20 and 40 μmol/L GA, respectively. Consistent results were observed when A549 cells were treated with the RAS inhibitor Tip (Fig. 4D and E). Previous results show that RAS is active between G0 and S phases of the cell cycle[46,47]. Previous results show that RAS activity is required for both cell cycle initiation and subsequent G1 progression through the activation of various RAS effector pathways[48,49]. In order to explore whether the cell cycle arrest contributed to GA-induced proliferation inhibition, we further analysed the cell cycle distribution, and we found that GA induced S phase arrest in A549 cells (Fig. 4F and G).

3.6. *GA inhibits tumour growth in the mouse xenograft model*

The antitumour activity of GA was assessed using a xenograft of A549 cells in nude mice. The tumour size of the model group displayed a significant increase compared with the GA-treated mice (Fig. 5A and B). A high dose of GA inhibited tumour growth by
50%–60%, similar to animals treated with Kobe[29]. For the histological analysis, tumour tissue sections were stained with haematoxylin & eosin (H&E). Compared with the model group, the high-dose GA and Kobe groups exhibited an obviously ameliorated severity of necrosis and pyknosis in the nuclei of tumour cells. Immunohistochemistry (IHC) of the tumour tissue revealed a substantial decrease in ERK1/2 phosphorylation of ERK1/2 in response to the GA treatment (Fig. 5C). Furthermore, we tested the expression of phospho-c-RAF, phospho-B-RAF and phospho-ERK1/2 in the tumour tissues from both the GA- and Kobe-treated groups. The level of phosphorylation of c-RAF at Ser259, B-RAF at both Ser729 and Thr401, ERK1/2 was decreased following GA treatment high-dose group. (Fig. 5D and E).

4. Discussion

Here, our study demonstrates that GA acts as a ligand targeting the P-loop of the RAS protein. They are identified by chemical biology strategies and biophysical techniques. P-loop is a conserved sequence motif (GxxxxGKS/T) found in the superfamily of P-loop nucleoside triphosphate hydrolases (NTPases)[50]. In generally, all GTPases are involved in signal transduction and regulation belongs to P-loop NTPases[51]. The P-loop maintains the GTP in an appropriate configuration for nucleophilic attack by a water molecule interacting with the switch I and II regions[52]. GDP–GTP exchange is mainly regulated by GEFs, which assist in displacing the bound GDP and replacing it with GTP, and by GAPs, which are responsible for catalysing GTP hydrolysis[9]. Conformational changes in the P-loop may be a common strategy contributing to GEF-stimulated nucleotide exchange in G-proteins. Thus, Structural disruption of the P-loop is likely the essential mechanism underlying the sharply reduced catalytic function of GEFs for GDP release and GDP–GTP exchange[53], which leads to changes in affinity and kinetics of interaction with effectors.

According to us results of *in silico* docking and biophysical techniques results, GA is predicted to bind P-loop and switch II of

RAS which are composed of certain basic residues (G12, G13, V14, G15 and G60). Replacement of G12, G13 and G15 with alanine leaded to obvious loss of binding ability of GA, and these residues involved in GA-induced irregular oligomers. Studies have demonstrated that the switch I and II domains bind to γ-phosphate *via* the backbone NH groups of the invariant T35 and G60 residues, which may be referred to as the loading spring mechanism[8]. Release of the γ-phosphate after GTP hydrolysis allows the switch regions to relax into a different conformation. We hypothesized that GA binds to the P-loop region of the RAS protein, and release of γ-phosphate after normal GTP hydrolysis allows the two switch regions to relax into a GDP-specific conformation that is disturbed. A possible explanation for this phenomenon is that the GA exhausts the pool of GTP-RAS over time by promoting the intrinsic hydrolysis of bound GTP and simultaneously preventing the reactivation of GTP *via* GEF-catalysed GDP–GTP exchange. According to the results of FTS assay, the thermal stability of RAS protein was reduced by GA as it caused a 6–8 °C decrease in ΔT_m. In contrast to competitive inhibitors, GA exhibits the characteristics of an allosteric inhibitor. At present, the inhibitor SCH54292 was designed to directly block RAS by competing with nucleotides and binding to RAS, which revealed a new binding site, Lys101, under switch II[54]. A series of small-molecule compounds were administered to inhibit intrinsic nucleotide exchange, similar to the RAS neutralizing antibody Y13–259, which binds to amino acid residues in switch II (Glu-63, Ser-65, Ala-66, Met-67, and Arg-73)[55]. A natural product, andrographolide, and its derivatives bind to switch II (Tyr 64 and Tyr 71) and impair its interaction with RAS, thereby preventing GEF-assisted nucleotide exchange[19].

In cell signaling networks, the involvement of H-RAS, N-RAS or K-RAS in the RAS-RAF-MAPK pathway has shown to be critical for controlling proliferation, differentiation and survival[56,57]. Based on our intracellular enzyme activity and effector protein assay results, the activity of RAS decreased following the addition of 40 μmol/L GA. The level of phosphorylation c-RAF at both Ser338 and Ser259 sites decreased following GA treatment in a dose-dependent manner. We performed *in vitro* and *in vivo* studies to determine the effects of GA on tumor cell migration, invasion, and cell cycle progression using A549 cells and nude mice. GA successfully reduced tumor cell migration and invasiveness and inhibited cell cycle progression, thereby inhibiting the RAS/MAPK signalling pathway and associated downstream effectors RAF and ERK. The above results are consistent with previous reports that GA-treated tumor cells exhibit down-regulation of H-RAS protein, which affects cell cycle arrest and cell growth inhibition[58].

Naturally occurring triterpenoid saponin and its derivatives, such as, ursolic acid[59], including GA[60] have displayed a broad spectrum of anticancer activity and low toxicity. However, the identification of its precise anti-tumour targets is still challenging[61]. In contrast to competitive inhibitors, GA exhibits the characteristics of an allosteric inhibitor in our study. GA exerts an inhibitory effect by changing the conformation of the RAS protein. GA may be an effective and comparatively safe compound for the design and development of RAS-related antineoplastic drugs.

Acknowledgments

This work was supported by grants from National Natural Science Foundation of China (Grant Nos. 81430095, 81673616, and 81473403); and International Cooperation and Exchange of the National Natural Science Foundation of China (Grant No. 81761168039).

Appendix A. Supporting information

Supplementary data associated with this article can be found in the online version at https://doi.org/10.1016/j.apsb.2018.11.002.

References

1. Cox AD, Der CJ. Ras history: the saga continues. *Small GTPases* 2010;**1**:2–27.
2. Karnoub AE, Weinberg RA. Ras oncogenes: split personalities. *Nat Rev Mol Cell Biol* 2008;**9**:517–31.
3. Pylayeva-Gupta Y, Grabocka E, Bar-Sagi D. RAS oncogenes: weaving a tumorigenic web. *Nat Rev Cancer* 2011;**11**:761–74.
4. Stieglitz B, Bee C, Schwarz D, Yildiz O, Moshnikova A, Khokhlatchev A, et al. Novel type of Ras effector interaction established between tumour suppressor NORE1A and Ras switch II. *EMBO J* 2008;**27**:1995–2005.
5. Scheffzek K, Ahmadian MR, Kabsch W, Wiesmuller L, Lautwein A, Schmitz F, et al. The Ras–RasGAP complex: structural basis for GTPase activation and its loss in oncogenic Ras mutants. *Science* 1997;**277**:333–8.
6. Harrison RA, Lu J, Carrasco M, Hunter J, Manandhar A, Gondi S, et al. Structural dynamics in Ras and related proteins upon uucleotide switching. *J Mol Biol* 2016;**428**:4723–35.
7. Mueller MP, Goody RS. Review: Ras GTPases and myosin: qualitative conservation and quantitative diversification in signal and energy transduction. *Biopolymers* 2016;**105**:422–30.
8. Vetter IR, Wittinghofer A. The guanine nucleotide-binding switch in three dimensions. *Science* 2001;**294**:1299–304.
9. McCormick F. Ras GTPase activating protein: signal transmitter and signal terminator. *Cell* 1989;**56**:5–8.
10. Bonfini L, Karlovich CA, Dasgupta C, Banerjee U. The Son of sevenless gene product: a putative activator of Ras. *Science* 1992;**255**:603–6.
11. Spiegel J, Cromm PM, Zimmermann G, Grossmann TN, Waldmann H. Small-molecule modulation of Ras signaling. *Nat Chem Biol* 2014;**10**:613–22.
12. Schubbert S, Shannon K, Bollag G. Hyperactive Ras in developmental disorders and cancer. *Nat Rev Cancer* 2007;**7**:295–308.
13. Castellano E, Downward J. RAS interaction with PI3K: more than just another effector pathway. *Genes cancer* 2011;**2**:261–74.
14. Kolch W. Meaningful relationships: the regulation of the Ras/Raf/MEK/ERK pathway by protein interactions. *Biochem J* 2000;**351 Pt 2**:289–305.
15. Ferro E, Trabalzini L. RalGDS family members couple Ras to Ral signalling and that's not all. *Cell Signal* 2010;**22**:1804–10.
16. Roberts PJ, Der CJ. Targeting the Raf-MEK-ERK mitogen-activated protein kinase cascade for the treatment of cancer. *Oncogene* 2007;**26**:3291–310.
17. Wang W, Fang G, Rudolph J. Ras inhibition *via* direct Ras binding—is there a path forward?. *Bioorg Med Chem Lett* 2012;**22**:5766–76.
18. Downward J. Targeting RAS signalling pathways in cancer therapy. *Nat Rev Cancer* 2003;**3**:11–22.
19. Hocker HJ, Cho KJ, Chen CY, Rambahal N, Sagineedu SR, Shaari K, et al. Andrographolide derivatives inhibit guanine nucleotide exchange and abrogate oncogenic Ras function. *Proc Natl Acad Sci U S A* 2013;**110**:10201–6.
20. Hunter JC, Gurbani D, Ficarro SB, Carrasco MA, Lim SM, Choi HG, et al. *In situ* selectivity profiling and crystal structure of SML-8-73-1, an active site inhibitor of oncogenic K-Ras G12C. *Proc Natl Acad Sci U S A* 2014;**111**:8895–900.
21. Gentile DR, Rathinaswamy MK, Jenkins ML, Moss SM, Siempelkamp BD, Renslo AR, et al. Ras binder induces a modified switch-II pocket in GTP and GDP states. *Cell Chem Biol* 2017;**24:** 1455-66. e14.

22. Cox AD, Der CJ, Philips MR. Targeting RAS membrane association: back to the future for anti-RAS drug discovery?. *Clin Cancer Res* 2015;**21**:1819–27.
23. Zimmermann G, Papke B, Ismail S, Vartak N, Chandra A, Hoffmann M, et al. Small molecule inhibition of the KRAS-PDEδ interaction impairs oncogenic KRAS signalling. *Nature* 2013;**497**:638–42.
24. Akasaka Y, Yoshida T, Tsukahara M, Hatta A, Inoue H. Glycyrrhetinic acid prevents cutaneous scratching behavior in mice elicited by substance P or PAR-2 agonist. *Eur J Pharmacol* 2011;**670**:175–9.
25. Wang L, Yang R, Yuan B, Liu Y, Liu C. The antiviral and antimicrobial activities of licorice, a widely-used Chinese herb. *Acta Pharm Sin B* 2015;**5**:310–5.
26. Csuk R, Schwarz S, Siewert B, Kluge R, Strohl D. Conversions at C-30 of glycyrrhetinic acid and their impact on antitumor activity. *Arch Pharm* 2012;**345**:223–30.
27. Shi Q, Hou Y, Hou J, Pan P, Liu Z, Jiang M, et al. Glycyrrhetic acid synergistically enhances β_2-adrenergic receptor-Gs signaling by changing the location of Galphas in lipid rafts. *PLoS One* 2012;**7**:e44921.
28. Fang R, Cui Q, Sun J, Duan X, Ma X, Wang W, et al. PDK1/Akt/PDE4D axis identified as a target for asthma remedy synergistic with β2 AR agonists by a natural agent arctigenin. *Allergy* 2015;**70**:1622–32.
29. Shima F, Yoshikawa Y, Ye M, Araki M, Matsumoto S, Liao J, et al. *In silico* discovery of small-molecule Ras inhibitors that display antitumor activity by blocking the Ras-effector interaction. *Proc Natl Acad Sci U S A* 2013;**110**:8182–7.
30. Sparano JA, Moulder S, Kazi A, Coppola D, Negassa A, Vahdat L, et al. Phase II trial of tipifarnib plus neoadjuvant doxorubicin–cyclophosphamide in patients with clinical stage IIB-IIIC breast cancer. *Clin Cancer Res* 2009;**15**:2942–8.
31. Fu X, Wang Z, Li L, Dong S, Li Z, Jiang Z, et al. Novel chemical ligands to Ebola virus and Marburg virus nucleoproteins identified by combining affinity mass spectrometry and metabolomics approaches. *Sci Rep* 2016;**6**:29680.
32. Chen PH, Unger V, He X. Structure of full-length human PDGFRβ bound to its activating ligand PDGF-B as determined by negative-stain electron microscopy. *J Mol Biol* 2015;**427**:3921–34.
33. Wei Y, Yang Q, Zhang Y, Zhao T, Liu X, Zhong J, et al. Plumbagin restrains hepatocellular carcinoma angiogenesis by suppressing the migration and invasion of tumor-derived vascular endothelial cells. *Oncotarget* 2017;**8**:15230–41.
34. Lo MC, Aulabaugh A, Jin G, Cowling R, Bard J, Malamas M, et al. Evaluation of fluorescence-based thermal shift assays for hit identification in drug discovery. *Anal Biochem* 2004;**332**:153–9.
35. Kelly SM, Price NC. The application of circular dichroism to studies of protein folding and unfolding. *Biochim Biophys Acta* 1997;**1338**:161–85.
36. Wittinghofer A, Vetter IR. Structure–function relationships of the G domain, a canonical switch motif. *Annu Rev Biochem* 2011;**80**:943–71.
37. Kinoshita K, Sadanami K, Kidera A, Go N. Structural motif of phosphate-binding site common to various protein superfamilies: all-against-all structural comparison of protein-mononucleotide complexes. *Protein Eng* 1999;**12**:11–4.
38. Xiao J, Xing F, Liu Y, Lv Y, Wang X, Ling MT, et al. Garlic-derived compound *S*-allylmercaptocysteine inhibits hepatocarcinogenesis through targeting LRP6/Wnt pathway. *Acta Pharm Sin B* 2018;**8**:575–86.
39. Chatellier J, Mazza A, Brousseau R, Vernet T. Codon-based combinatorial alanine scanning site-directed mutagenesis: design, implementation, and polymerase chain reaction screening. *Anal Biochem* 1995;**229**:282–90.
40. Singh H, Longo DL, Chabner BA. Improving prospects for targeting RAS. *J Clin Oncol* 2015;**33**:3650–9.
41. Hou Y, Nie Y, Cheng B, Tao J, Ma X, Jiang M, et al. Qingfei Xiaoyan Wan, a traditional Chinese medicine formula, ameliorates *Pseudomonas aeruginosa*-induced acute lung inflammation by regulation of PI3K/AKT and Ras/MAPK pathways. *Acta Pharm Sin B* 2016;**6**:212–21.
42. Liu F, Yang X, Geng M, Huang M. Targeting ERK, an Achilles' Heel of the MAPK pathway, in cancer therapy. *Acta Pharm Sin B* 2018;**8**:552–62.
43. Moodie SA, Willumsen BM, Weber MJ, Wolfman A. Complexes of Ras.GTP with Raf-1 and mitogen-activated protein kinase kinase. *Science* 1993;**260**:1658–61.
44. Zhang XF, Settleman J, Kyriakis JM, Takeuchi-Suzuki E, Elledge SJ, Marshall MS, et al. Normal and oncogenic p21ras proteins bind to the amino-terminal regulatory domain of c-Raf-1. *Nature* 1993;**364**:308–13.
45. Watanabe M, Miyajima N, Igarashi M, Endo Y, Watanabe N, Sugano S. Sodium phenylacetate inhibits the Ras/MAPK signaling pathway to induce reduction of the c-Raf-1 protein in human and canine breast cancer cells. *Breast Cancer Res Treat* 2009;**118**:281–91.
46. Feig LA, Cooper GM. Inhibition of NIH 3T3 cell proliferation by a mutant ras protein with preferential affinity for GDP. *Mol Cell Biol* 1988;**8**:3235–43.
47. Dobrowolski S, Harter M, Stacey DW. Cellular ras activity is required for passage through multiple points of the G0/G1 phase in BALB/c 3T3 cells. *Mol Cell Biol* 1994;**14**:5441–9.
48. Jones SM, Kazlauskas A. Growth-factor-dependent mitogenesis requires two distinct phases of signalling. *Nat Cell Biol* 2001;**3**:165–72.
49. Kumar A, Marques M, Carrera AC. Phosphoinositide 3-kinase activation in late G1 is required for c-Myc stabilization and S phase entry. *Mol Cell Biol* 2006;**26**:9116–25.
50. Wilson D, Madera M, Vogel C, Chothia C, Gough J. The SUPERFAMILY database in 2007: families and functions. *Nucleic Acids Res* 2007;**35**:D308–13.
51. Leipe DD, Wolf YI, Koonin EV, Aravind L. Classification and evolution of P-loop GTPases and related ATPases. *J Mol Biol* 2002;**317**:41–72.
52. Ostrem JM, Peters U, Sos ML, Wells JA, Shokat KM. K-Ras (G12C) inhibitors allosterically control GTP affinity and effector interactions. *Nature* 2013;**503**:548–51.
53. Mercier E, Girodat D, Wieden HJ. A conserved P-loop anchor limits the structural dynamics that mediate nucleotide dissociation in EF-Tu. *Sci Rep* 2015;**5**:7677.
54. Ganguly AK, Pramanik BN, Huang EC, Liberles S, Heimark L, Liu YH, et al. Detection and structural characterization of ras oncoprotein-inhibitors complexes by electrospray mass spectrometry. *Bioorg Med Chem* 1997;**5**:817–20.
55. Hattori S, Clanton DJ, Satoh T, Nakamura S, Kaziro Y, Kawakita M, et al. Neutralizing monoclonal antibody against ras oncogene product p21 which impairs guanine nucleotide exchange. *Mol Cell Biol* 1987;**7**:1999–2002.
56. Der CJ, Krontiris TG, Cooper GM. Transforming genes of human bladder and lung carcinoma cell lines are homologous to the ras genes of *Harvey* and *Kirsten sarcoma* viruses. *Proc Natl Acad Sci U S A* 1982;**79**:3637–40.
57. Parada LF, Tabin CJ, Shih C, Weinberg RA. Human EJ bladder carcinoma oncogene is homologue of *Harvey sarcoma* virus ras gene. *Nature* 1982;**297**:474–8.
58. Yu T, Yamaguchi H, Noshita T, Kidachi Y, Umetsu H, Ryoyama K. Selective cytotoxicity of glycyrrhetinic acid against tumorigenic r/m HM-SFME-1 cells: potential involvement of H-Ras downregulation. *Toxicol Lett* 2010;**192**:425–30.
59. Mendes VIS, Bartholomeusz GA, Ayres M, Gandhi V, Salvador JA. Synthesis and cytotoxic activity of novel A-ring cleaved ursolic acid derivatives in human non-small cell lung cancer cells. *Eur J Med Chem* 2016;**123**:317–31.
60. Tang ZH, Zhang LL, Li T, Lu JH, Ma DL, Leung CH, et al. Glycyrrhetinic acid induces cytoprotective autophagy *via* the inositol-requiring enzyme 1α-c-Jun N-terminal kinase cascade in non-small cell lung cancer cells. *Oncotarget* 2015;**6**:43911–26.
61. Qi LW, Wang CZ, Yuan CS. Isolation and analysis of ginseng: advances and challenges. *Nat Prod Rep* 2011;**28**:467–95.